II

Petri Kanninen, Maryam Borghei, Virginia Ruiz, Esko I. Kauppinen, Tanja Kallio: The effect of Nafion content in graphitized carbon nanofiber based anode for the direct methanol fuel cell, Int. J. Hydrogen Energy 37 (2012) 19082-19091.

INTERNATIONAL JOURNAL OF HYDROGEN ENERGY 37 (2012) 19082–19091

Available online at www.sciencedirect.com

SciVerse ScienceDirect

journal homepage: www.elsevier.com/locate/he

The effect of Nafion content in a graphitized carbon nanofiber-based anode for the direct methanol fuel cell

Petri Kanninen [a], Maryam Borghei [b], Virginia Ruiz [b,c], Esko I. Kauppinen [b], Tanja Kallio [a,*]

[a] Department of Chemistry, Aalto University, Helsinki, P.O. Box 16100, FI-00076 Aalto, Finland
[b] Department of Applied Physics, Aalto University, P.O. Box 15100, FI-00076 Aalto, Finland
[c] IK4-CIDETEC – Centre for Electrochemical Technologies, Paseo Miramón 196, E-20009 Donostia-San Sebastián, Spain

ARTICLE INFO

Article history:
Received 5 July 2012
Received in revised form
21 September 2012
Accepted 23 September 2012
Available online 22 October 2012

Keywords:
Direct methanol fuel cell
Carbon nanofiber
Nafion
Ionomer content
Anode structure
Durability

ABSTRACT

The performance and stability of a direct methanol fuel cell (DMFC) with membrane electrode assemblies (MEA) using different Nafion® contents (30, 50 and 70 wt% or MEA30, MEA50 and MEA70, respectively) and graphitized carbon nanofiber (GNF) supported PtRu catalyst at the anode was investigated by a constant current measurement of 9 days (230 h) in a DMFC and characterization with various techniques before and after this measurement. Of the pristine MEAs, MEA50 reached the highest power and current densities. During the 9-day measurement at a constant current, the performance of MEA30 decreased the most ($-124\ \mu V\ h^{-1}$), while the MEA50 was almost stable ($-11\ \mu V\ h^{-1}$) and performance of MEA70 improved ($+115\ \mu V\ h^{-1}$). After the measurement, the MEA50 remained the best MEA in terms of performance. The optimum anode Nafion content for commercial Vulcan carbon black supported PtRu catalysts is between 20 and 40 wt%, so the GNF-supported catalyst requires more Nafion to reach its peak power. This difference is explained by the tubular geometry of the catalyst support, which requires more Nafion to form a penetrating proton conductive network than the spherical Vulcan. Mass transfer limitations are mitigated by the porous 3D structure of the GNF catalyst layer and possible changes in the compact Nafion filled catalyst layers during constant current production.

1. Introduction

Liquid-fed fuel cells, like the direct methanol fuel cell (DMFC), are a very promising candidate for power sources of low-power electronic devices. However, breaking out from the niche market requires improvements in the performance, durability and cost of the catalysts [1] and membranes [2]. A crucial limitation of the DMFC is the catalysis of the methanol oxidation reaction at the anode. Currently widely used PtRu catalyst (pure or carbon supported) requires high loading leading to high cost and durability issues due to the dissolution of Ru under fuel cell conditions. Two common approaches for the improvement of the catalyst activity, cost and stability are the modification of the active metals or the modification of the conductive carbon support.

The basic requirements for the catalyst support are high surface area for the metal catalyst nanoparticle deposition, good permeability for the reactants and products, stability in the chemical and electrochemical conditions in the fuel cell and high electronic conductivity. Due to their appealing properties in this regard, many alternative carbon nanostructures have been explored to replace the carbon black

* *Corresponding author*. Tel.: +358 9470 22583; fax: +358 9470 22580.
E-mail address: tanja.kallio@aalto.fi (T. Kallio).
0360-3199/$ – see front matter
http://dx.doi.org/10.1016/j.ijhydene.2012.09.138

usually employed as the catalyst support [3]: single-walled [4,5] and multi-walled [6–8] carbon nanotubes, graphitized carbon nanofibers [9], fullerenes [10,11], carbon nanohorns [12] and mesoporous carbon [13,14].

Specifically, graphitized carbon nanofibers (GNF) have high electronic conductivity and thermal oxidation resistance due to their graphitic nature [15,16] as well as high mesoporous content, which can enhance mass transfer through the catalyst layer [17,18]. Also, it has been suggested [19] that the high electrochemical capacitances of edge-rich GNF types (herringbone and platelet) [20] indicate strong interactions with ions and this would stabilize metallic catalyst particles formed from ions on these surfaces. Finally, GNF-supported Pt and PtRu catalysts have shown improved activity and stability toward methanol and CO oxidation [18,21–23].

It is important to test new catalysts under fuel cell conditions. If the only tests are for catalytic activity in a half-cell electrochemical set-up, the conditions will not accurately reproduce the situation in a fuel cell. This is because there is no fabrication of the membrane electrode assembly (MEA), whose properties are vital to the functionality of the fuel cell, and the long-term stability of the catalyst usually remains unknown. Therefore, GNF-supported PtRu has been used in various DMFC experiments as the anode catalyst [19,24–26].

Steigerwalt et al. [24] showed that a herringbone type GNF-PtRu performed 64% better than a colloidal PtRu black at low catalyst loading. Guo et al. [25] studied reduced and oxidized herringbone GNF-PtRu and found that while PtRu deposited more smoothly on the reduced GNF, the DMFC performance was better with the oxidized GNF with the overall performances of the both GNF types being better than the commercial carbon black supported PtRu. On the other hand, Tsuji et al. [26] determined that in the DMFC, a platelet type GNF-PtRu was superior in comparison with a herringbone and a tubular GNF-PtRu. All the GNF materials performed clearly better than the commercial alternative in the DMFC. Kang et al. [19] studied the long-term stability of a herringbone GNF-PtRu in a DMFC for 2000 h. It was found that the voltage decay was 30% smaller for the GNF-PtRu and metal dissolution was also slower than for a commercial activated carbon supported PtRu, though the DMFC performance was similar for both cases.

Pure GNF without a metal catalyst have also been used to modify the properties of the MEA. Okada et al. [27] fabricated a GNF interlayer between the catalyst layer and the gas diffusion layer, which could be used to tailor the mass-transport between the layers. Park et al. [28] used GNF as an additive in the anode carbon black PtRu catalyst layer to enhance the mass-transport. Higher porosity and electrochemically active surface area were measured at the anode, which led to smaller overvoltage and better performance in a DMFC.

When the properties of the carbon support change, it is also probable that the optimum fuel cell catalyst layer structure changes. For example, carbon nanofibers and nanotubes have a long and thin geometry as well as different porosity and electronic structure when compared with traditional carbon black. However, when new carbon supported catalysts are tested in fuel cells, the usual approach is to use optimum compositions found for commercial carbon black (Vulcan) catalysts. The optimum ionomer-carbon ratio for these catalysts has been studied several times for DMFC MEAs in the past [29–32]. The optimum depends on the exact metal to carbon ratio and the method of MEA fabrication, but it is usually between 25 and 40 wt% of the total dry mass of the electrode. If a pure PtRu black catalyst without support is used, the optimum is between 10 and 20 wt% [33–36] as the pure metal is more compact and requires less Nafion to form a penetrating network. This confirms the intuitive idea that the catalyst structure affects the optimum MEA structure and component ratios. For new alternative supports, little optimization of the DMFC electrode structure has been made. To the authors' best knowledge, the only study is by Jeng et al. [37], who investigated the optimum Nafion content of PtRu supported on multi-walled carbon nanotubes and found that 62 wt% of Nafion on the anode resulted in the best performance. This indicates that the different shape and structure of the catalyst support may cause significant differences in the optimum Nafion content and it should be determined for each case. For hydrogen fed polymer electrolyte fuel cells, a similar finding has been reported for GNF-Pt catalyst on the cathode, where 50 wt% Nafion performed better than 30 wt% Nafion [38]. When both the anode and cathode were studied simultaneously, optimum performance was reached with 30 wt% Nafion in both the anode and the cathode catalyst layer.

In our recent publication [23], a systematic comparison of PtRu supported by three different carbon nanosupports (Vulcan, few-walled carbon nanotubes and GNF) was conducted. The results indicated that the GNF-supported PtRu exhibits better stability but poorer performance compared with the commercial Vulcan support under fuel cell conditions. However, the Nafion content used for the three types of nanocarbons was the optimum for Vulcan supported catalysts. In this study, PtRu catalyst with the same GNF support was used to fabricate the anode of DMFC MEAs with different Nafion content. The performance and stability of the MEAs were studied with different techniques before, during and after a 9-day (230 h) constant current measurement.

2. Experimental

2.1. *Catalyst material preparation*

Graphitized carbon nanofibers (GNF, from Showa Denko Co. Ltd.) were subjected to an annealing process at ~2000 °C to achieve a high degree of graphitization. After annealing the GNF were treated with a mixture of 2 M HNO_3/1 M H_2SO_4 (1:1 v:v) and refluxed at 120 °C for 4 h in order to introduce active sites on the fiber walls for anchoring catalyst particles by oxidative functionalization. These GNFs with a diameter and length of about 150 nm and 8 μm, respectively, were then used as a carbon support material.

The GNF-supported PtRu was synthesized by reduction of Pt and Ru precursors via the polyol method. Firstly, GNF were mixed with ethylene glycol (EG) and ultrasonicated for 30 min. The required amount of Pt (K_2PtCl_6) and Ru ($RuCl_3$) precursors (Pt:Ru atomic ratio of 1:1 and metal loading of 30 wt%) were mixed in a solution containing EG and water and placed in an

ultrasound bath for 30 min. It was then added dropwise to the GNF-EG solution and ultrasonicated for a further 30 min to get a homogeneous solution. After that, a solution consisting of 0.04 M $NaBH_4$ and 0.005 M NaOH was added dropwise and the resulting suspension was ultrasonicated at 50 °C for 2 h to ensure complete reduction. Finally, the suspension was filtered and the solid product was collected, washed thoroughly with deionized water and dried in vacuum at 40 °C overnight.

2.2. MEA preparation

A Nafion 115 membrane was cleaned by boiling sequentially in 5 wt% H_2O_2, 0.5 M H_2SO_4 and three times in deionized water. It was then dried in a vacuum oven at 80 °C for 2 h and weighed. The catalyst ink was prepared by mixing the catalyst (60 wt% Pt on Vulcan (Alfa Aesar) for the cathode and the synthesized 30 wt% PtRu on GNF for the anode) with 5 wt% Nafion dispersion (Aldrich). Isopropanol and water were used as additional solvents to control the viscosity. The components were mixed by a magnetic stirrer for several hours and the Vulcan ink was subjected to additional sonication by an ultrasonic bath. The resulting slurry was painted on the Nafion 115 membrane by an air brush and dried in a vacuum oven at 80 °C for 2 h. The MEA was then weighed to determine the weight of the dry catalyst layer. Four types of MEAs were made, each with a different Nafion content in the anode catalyst layer: 30, 50, 70 and 90 wt% and these were designated as MEA30, MEA50, MEA70 and MEA90. The large amount of the Nafion dispersion in the MEA90 anode made it unsuitable for the fabrication method employed and thus it was not studied further. The PtRu loadings for each successfully fabricated anode were as follows (in $mg\,cm^{-2}$): 0.40 (MEA30), 0.52 (MEA50) and 0.44 (MEA70). The cathode Pt loading was approximately 1 $mg\,cm^{-2}$ in each MEA to ensure that it did not limit the performance. Finally, the MEA was heat pressed at 130 °C with 50 bar pressure for 2 min.

2.3. Characterization of the catalyst layer

Transmission electron microscopy (TEM) was carried out with a Tecnai 12 Bio Twin transmission electron microscope with a LaB_6 gun at 80 kV to characterize the synthesized GNF-PtRu catalyst.

Powder X-ray diffraction (XRD) spectra were obtained by a Bruker D8 Advance X-ray diffractometer using Cu Kα radiation and a Lynx Eye fast detector with scan conditions of 2 s/0.03°. The spectra were measured directly from the anode catalyst layer of the pristine and used MEAs without removing the catalyst from the membrane.

Scanning electron microscopy (SEM) was performed on a JEOL JSM-7500FA field emission scanning electron microscope equipped with an energy-dispersive X-ray spectrometer (EDXS). For cross-section imaging, the MEAs were frozen in liquid nitrogen to allow the samples to be easily cut with minimal damage to the MEA structure. An average thickness was determined by measuring at four different locations across the sample.

Contact angle measurements were made using a KSV Instruments CAM200 optical tensiometer. Before the measurement, the MEAs were first boiled in deionized water for 10 min, cooled down and stored in the water to ensure a completely wetted catalyst layer to eliminate the distorting effect water has on dry Nafion [39]. The membrane was taken out of water, patted dry on the surface and a static contact angle measurement was made immediately. The contact angle was measured at three locations on the anode of each MEA to produce an average with the MEA being allowed to rehydrate between each measurement.

The resistance of the catalyst layer was measured in a four-probe conductivity cell (BekkTech). The measurement was made in-plane across the catalyst layer by sweeping potential from 0 to 1 V at a scan rate of 20 $mV\,s^{-1}$ with a Metrohm Autolab PGSTAT100. The resistance was then calculated from the slope of the line fitted to the voltage–current plot of the data.

The specific surface areas of the MEAs were obtained by a micromeritics FlowSorb II 2300 N_2 adsorption/desorption apparatus. The MEA sample holder was placed in liquid N_2 (77 K), while gaseous N_2 was flowing through the cell. After 10 min of stabilization, the sample was heated to room temperature and the volume of the desorped N_2 was measured. The same method was used to determine the surface area of the GNF-PtRu catalyst.

2.4. Fuel cell experiments

The fuel cell was assembled with Teflon® gaskets, carbon cloth gas diffusion layers and an MEA. The cell was then clamped together with eight screws and tightened to a torque of 10 Nm. The active area of the fuel cell was 7.29 cm^2. Cell voltage and current were controlled by a Metrohm Autolab PGSTAT20 potentiostat with a BSTR10A booster. Prior to the measurement, the cell was first allowed to stabilize overnight at 30 °C, with a 0.1 $ml\,min^{-1}$ flow of 1 M methanol solution in deionized water at the anode and 100 $ml\,min^{-1}$ flow dry O_2 (5.0, Aga) at the cathode.

Once stabilized, the electrochemically active surface area (EASA) of the anode was measured by CO-stripping method [40]. First, fully humidified N_2 and 5% H_2 in Ar were fed to the anode and the cathode, respectively. When the open circuit voltage was stable, the fuel cell potential was set to 0.1 V and N_2 was replaced with CO (2.0, Aga) for 30 min. Then N_2 was switched back for 30 min to flush the anode from excess CO. Finally, two consecutive cyclic voltammograms were made from 0.1 to 1.2 V. During the first cycle, the entire adsorbed CO is oxidized, while the second cycle serves as the baseline. The amount of CO is calculated from the transferred charge under the CO electro-oxidation peak and converted to area by using the value 420 $mC\,cm^{-2}$ for the oxidation of an adsorbed monolayer of CO on a PtRu surface [41]. It is worth noting that this figure is an approximation derived for a pure Pt surface as the exact nature of CO absorption on a Ru surface is yet unknown and thus, it should only be used to calculate the surface area for the comparison of catalysts with similar structure.

After the EASA measurement, the methanol solution was replaced at the anode (2 $ml\,min^{-1}$) and dry O_2 (200 $ml\,min^{-1}$) at the cathode and the temperature was raised to 70 °C. After 2 h of stabilization, polarization curves were measured with

a voltage sweep from the open circuit voltage (OCV) to 0.05 V at a rate of 0.5 mV s^{-1}. Finally, the impedance spectrum of the whole cell was measured at 27 mA cm^{-2} from 100 kHz to 10 mHz using a 10 mA sinusoidal signal.

The flow rates were then reduced to 0.3 ml min^{-1} and 100 ml min^{-1}, for the 1 M methanol and O_2 respectively and the cell was stabilized for 1 h prior to a 9-day (230 h) galvanostatic (27 mA cm^{-2}) measurement. After the galvanostatic testing, the polarization curve, the impedance spectrum and finally the EASA were measured to determine any changes in performance.

3. Results and discussion

3.1. *Characterization of the catalyst and the catalyst layer*

TEM images of the synthesized catalyst are presented in Fig. 1. The lower magnification image (Fig. 1A) illustrates how the metal catalyst clusters have been deposited over the nanofiber surface evenly and the higher magnification (Fig. 1B) shows the individual catalyst particles present within the clusters. The specific surface area of the catalyst is 16.9 $m^2 g^{-1}$ as was determined from 1-point BET N_2 desorption experiment.

XRD spectra have been measured from both the pristine and used anode catalyst layers and also from a pure Nafion 115 membrane (Fig. 2). The spectra show the characteristic PtRu alloy crystal faces at 40.0° (111), 46.4° (200), 68.1° (220) and 82.2° (311) (PDF-4+ 04-001-0112). The hexagonal carbon peak C(002) is visible at around 26° and the graphite C(004) peak around 54° while the other hexagonal carbon peaks C(100) at 42°, C(101) at 45° and graphite peak C(110) at 78° are overlapped with Nafion and PtRu peaks. Rest of the peaks around 45°, 58°, 65°, 70° and 78° are from the Nafion membrane as indicated by the pure Nafion 115 sample. The average size of the catalyst particles before and after the 9-day galvanostatic measurement has been estimated from the XRD spectrum of each MEA by the Scherrer equation using the Pt(111) peak at 40°. Direct determination of the size and the size distribution from the TEM images could not be done as the large amount of Nafion in the catalyst layer in MEA50 and MEA70 made the separation of the catalyst and Nafion impossible. The average catalyst particle diameter in the anode catalyst layer is 2.81 nm for the pristine MEA and 3.69, 3.36 and 3.60 nm for MEA30, MEA50 and MEA70 respectively. Particle size increase is usually observed in tested DMFC anodes [42], however, MEA50 shows the smallest increase indicating that it is a more stable environment for the catalyst in this respect.

SEM images of the pristine and used anode catalyst layers are presented in Fig. 3 and their respective thicknesses are listed in Table 1. The addition of Nafion affects the morphology of the catalyst layer rendering it denser as can be seen in Fig. 3A–F. MEA30 has clear voids in the structure (Fig. 3A, B), while MEA50 is much denser (Fig. 3C, D) and MEA70 seems completely compact (Fig. 3E, F). As the mass of the catalyst stays the same, so the thickness of the anode should become larger as the Nafion content increases for the MEAs investigated. However, the anode of the pristine MEA50 is significantly thinner than either the anode of the used MEA50 or the anode of the pristine MEA30. This indicates that the catalyst layer in MEA50 is more tightly packed but expands when it is used, but this change is small when compared to that previously observed for a Vulcan supported catalyst [23]. The differences in the thicknesses of the anodes of the pristine and used MEA30 and MEA70 are not significant, which highlights the mechanical stability of the GNF based catalyst layers and is in agreement with the results reported by Santasalo-Aarnio et al. [23].

In Table 1, the in-plane resistivity of each MEA is presented before and after the 9-day galvanostatic measurement. As the electronic resistivity of the pure Showa Denko GNF (10^{-4} Ω cm) [43] is much smaller than the ionic resistivity of Nafion (~10 Ω cm) [44], these results demonstrate how well the GNF network conducts electrons. Usually, the smaller amount of Nafion in the catalyst layer, the smaller the overall resistivity of the whole layer since contact between individual GNF is not hindered by Nafion layers of higher resistivity forming between them. However, the smallest resistivity is measured with MEA50, which has only 25% of the resistivity of MEA30 and 5% of MEA70. This may be explained both by the voids visible in MEA30 that will not conduct electricity (Fig. 3A, B) and the better dispersion of GNF into a larger amount of the Nafion dispersion during the MEA preparation phase. The role of Nafion as carbon nanomaterial dispersion stabilizer has previously been seen with single-walled carbon nanotubes

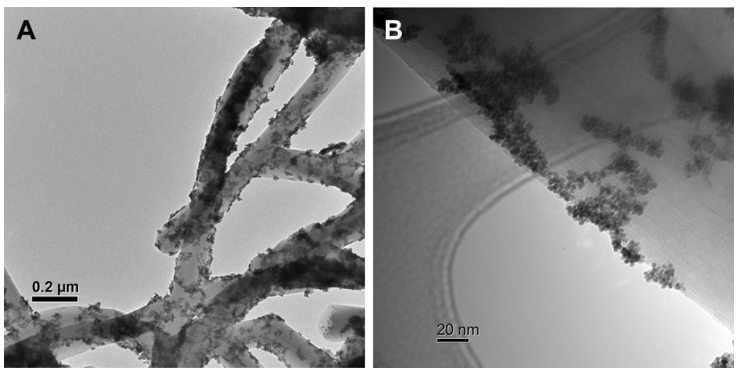

Fig. 1 – TEM images of the synthesized GNF-PtRu catalyst with a (A) lower and a (B) higher magnification.

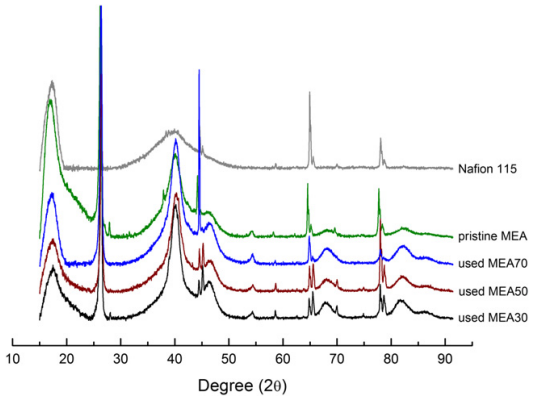

Fig. 2 – XRD spectra measured from the anode catalyst layers of the MEAs and pure Nafion 115 membrane. The pristine MEA was fabricated as the other MEAs with 50 wt% of Nafion in the anode catalyst layer.

[45]. With the GNF catalyst inks, a similar effect is observed as the ink becomes smoother as the amount of Nafion is increased. The better dispersion ensures that the GNF are distributed more evenly through the catalyst layer leading to the improved conductivity – in MEA50 the structure appears smoother with Nafion and GNF filling nearly the whole volume of the catalyst layer (Fig. 3C, D). It seems that around 50 wt% Nafion, the structure is optimized so that the GNF form a good network across the layer while the amount of Nafion is not large enough to hinder the conductivity. With MEA70, the resistivity is already much larger than with MEA30 and MEA50 indicating that at this concentration Nafion is blocking the GNF pathways.

The through-plane area resistance, determined from the high frequency end of the in-situ impedance spectroscopy of the fuel cell, revealed a similar order of resistances (Table 1). The differences between the MEAs are relatively smaller than with the in-plane measurements, because the resistance of the whole cell is measured and the membrane resistance tends to predominate. The area resistances decrease during the 9-day galvanostatic measurement in the same fashion as

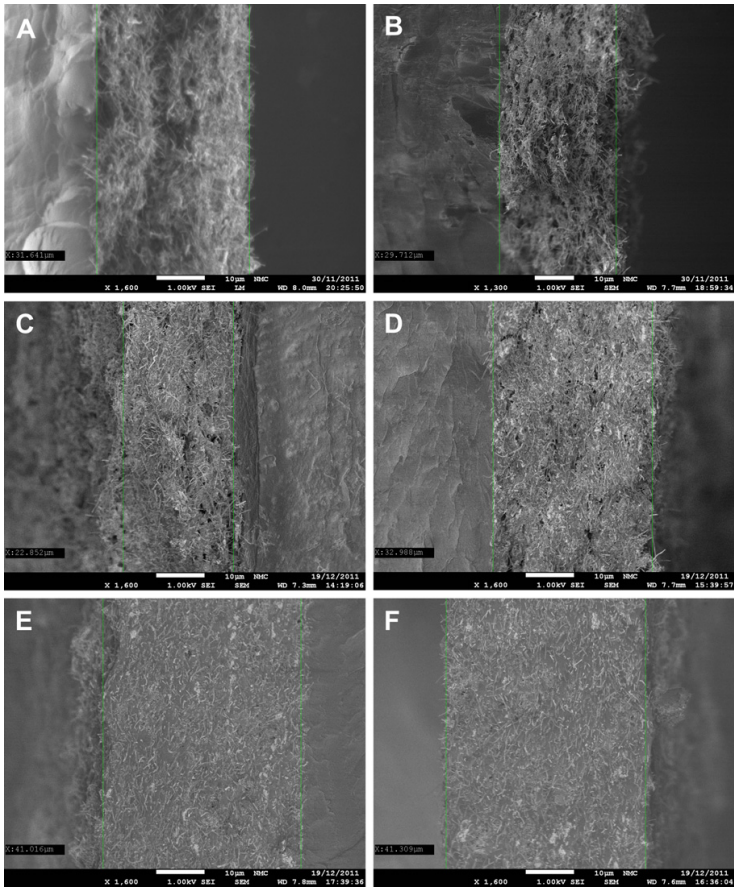

Fig. 3 – SEM images of pristine (A, C, E) and used (B, D, F) anode catalyst layers of (A, B) MEA30, (C, D) MEA50 and (E, F) MEA70 of Nafion.

Table 1 – The properties of the anode catalyst layer and the area resistance of the pristine and used MEAs.

	Thickness (μm)		Contact angle (°)		Resistivity (Ω cm) (in-plane)		Area resistance (Ω cm^2) (through-plane)	
	Pristine	Used	Pristine	Used	Pristine	Used	Pristine	Used
MEA30	32	30	158	159	0.35	0.20	0.19	0.14
MEA50	25	35	147	137	0.08	0.06	0.18	0.13
MEA70	44	41	112	104	1.40	1.19	0.22	0.19

in the ex-situ in-plane measurements and thus appear to reflect changes in the electrode structure. This whole cell impedance contains a significant number of elements that preclude any reliable equivalent circuit analysis.

In Table 1, contact angles for the anode catalyst layers of each MEA are presented. MEA30 exhibits superhydrophobic behavior (contact angle >150°) most likely due to its rough surface (Fig. 3A, B) and small Nafion content. MEA50 is still highly hydrophobic even though Nafion is already occupying more space in the catalyst layer, while with a further increase in Nafion content (MEA70) the surface becomes less hydrophobic. The contact angles of MEA50 are in the same range as the contact angles measured on commercial catalyst coated membranes for hydrogen polymer electrolyte fuel cells (144–150°) [46], while on the other hand, the contact angle on MEA70 (112°) is similar to that of a clean Nafion film hydrated at 90 °C (~110°) [47] indicating that Nafion is covering almost the whole surface of the catalyst layer. A hydrophobic nature of the catalyst layer is good for the removal of gaseous CO_2 produced through the oxidation of methanol, though a highly hydrophobic surface may prevent the proper wetting of the catalyst layer and the membrane leading to a decrease in their ionic conductivities. As a result, MEA50 could make a good compromise between the two properties by having enough hydrophobicity for efficient CO_2 removal and wettability for reasonable ionic conductivity. In the case of MEA50 and MEA70, the contact angle also shows a decrease of about 10° during the 9-day galvanostatic measurement, which could be due to the swelling of Nafion in methanol/water solution during the measurement. This may cause the GNF on the surface to be covered by Nafion more and thus decrease the contact angle. For MEA30, the Nafion content may have been too small and the surface too rough for this effect to be noticeable.

The specific surface areas of the MEAs measured by 1-point BET N_2 desorption experiments resulted in calculated specific surface areas (in $m^2 g^{-1}$) of 0.8 (MEA30), 0.7 (MEA50) and 0.3 (MEA70), whereas for a pure Nafion 115 sample value of 0.3 $m^2 g^{-1}$ was obtained. This indicates that the catalyst layers of MEA30 and MEA50 exhibit more porous character compared with that of MEA70 and that the surface area of MEA70 resembles a pure Nafion membrane.

3.2. *Fuel cell experiments*

As outlined previously, a 9-day (230 h) galvanostatic measurement at 27 mA cm^{-2} has been made with each MEA to assess their long-term stability (Fig. 4). Constant current has been used to ensure that each MEA is stressed in a similar manner by methanol oxidation products at the anode and H_2O production at the cathode. It can be seen from the results that the Nafion content has a notable effect on the long-term performance of the fuel cell. All MEAs show a rapid decline in voltage at the beginning of the measurement, which is likely due to concentration gradients forming in the electrodes, membrane and gas diffusion layer hydration, methanol crossover and other factors that will balance over time [48]. After approximately 20 h, the voltage change reaches a more stable region, the nature of which depends on the Nafion content. The voltage over MEA30 continues its decline almost until the end of the measurement. The performance of MEA50 is almost stable over the whole measurement period, while the voltage over MEA70 displays a steady increase after the initial drop stabilizes.

By calculating the change of voltage as the difference between the average potentials at time intervals 20–30 h and 220–230 h, the following results are obtained (in μV h^{-1}): −124 (MEA30), −11 (MEA50) and +115 (MEA70). It is clear that increasing the amount of Nafion in the anode catalyst layer results in a more stable fuel cell performance. The improving performance of MEA70 is interesting but would most likely start to level and decrease if measurement time would be lengthened. Kang et al. [19] reported degradation rates of −23 and −28 μV h^{-1} for their GNF-supported PtRu(40%) and PtRu(70%) catalysts during a 2000 h constant current measurement in a DMFC. They did not report the Nafion content of their GNF-PtRu anodes. All the measurements have a discontinuity point at around 110 h, which has been caused by a short pause (2 min) in the protocol resulting in the DMFC switching to OCV during this time. The increases in voltage indicate that a large part of

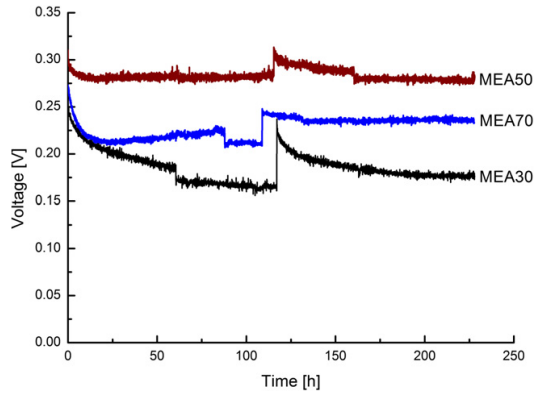

Fig. 4 – Nine-day (230 h) galvanostatic measurements at 27 mA cm^{-2} in a DMFC for MEA30 (black), MEA50 (red) and MEA70 (blue). (For interpretation of the references to color in this figure legend, the reader is referred to the web version of this article.)

the performance loss is reversible and that its effects can be mitigated by an on–off loading method [49], though the method has not been used here due to the limitations in the measurement software. The small drops in voltage at 55 (MEA30), 70 (MEA70) and 160 h (MEA50) are caused by the emptying of the exhaust water tank on the cathode side of the fuel cell. Overall as the amount of catalyst in each MEA varied slightly, these results should only be used to estimate the stability of each MEA and not the absolute performance.

Polarization curves have been measured from each MEA before and after the 9-day galvanostatic measurement. As the catalyst amount on each MEA anode varies slightly, both the curves for voltage (Fig. 5A, C) and the power density (Fig. 5B, D) are presented as normalized plots against either the active area (Fig. 5A, B) or total PtRu mass (Fig. 5C, D). As the active area has been the same in each measurement, the following discussion will concentrate on the data normalized against catalyst mass as it offers better comparability due to the fact that DMFC performance is linearly dependent on the PtRu loading [50]. Key values regarding the performance are presented in Table 2.

From Table 2, it can be seen that MEA50 showed the best performance of the pristine MEAs in terms of maximum power density (in mW mg^{-1}): 22.9 (MEA30), 24.4 (MEA50) and 21.9 (MEA70), and the same is also true for the current densities at 0.05 V (in mA mg^{-1}): 242 (MEA30), 283 (MEA50) and 216 (MEA70). Therefore performance-wise, the optimum anode Nafion content is higher than with the carbon black supported catalysts (25–40 wt%) [30–32], and lower than the optimum found for the multi-walled carbon nanotube supported catalysts (62 wt%) [37]. It appears that more Nafion is required to connect the active catalyst sites to the proton conducting network efficiently for the tubular GNF than for spherical carbon black, which is unexpected since the surface area is 13 $m^2 g^{-1}$ for the GNF and 250 $m^2 g^{-1}$ for Vulcan [3]. A probable explanation for this is the presence of great number of voids in the catalyst layer structure formed with the GNF (Fig. 2A, B). These voids need to be filled for an ion-conducting network to be formed through the layer. The catalyst layer structure formed by Vulcan is more compact and thus requires less Nafion to be impregnated [23] even though the surface area of the catalyst support is significantly larger. Multi-walled carbon nanotubes have a tubular geometry like GNF but form thick catalyst layers [23] and have a large surface area (200–400 $m^2 g^{-1}$) [3], which can explain the larger amount of Nafion required for optimum performance when compared to

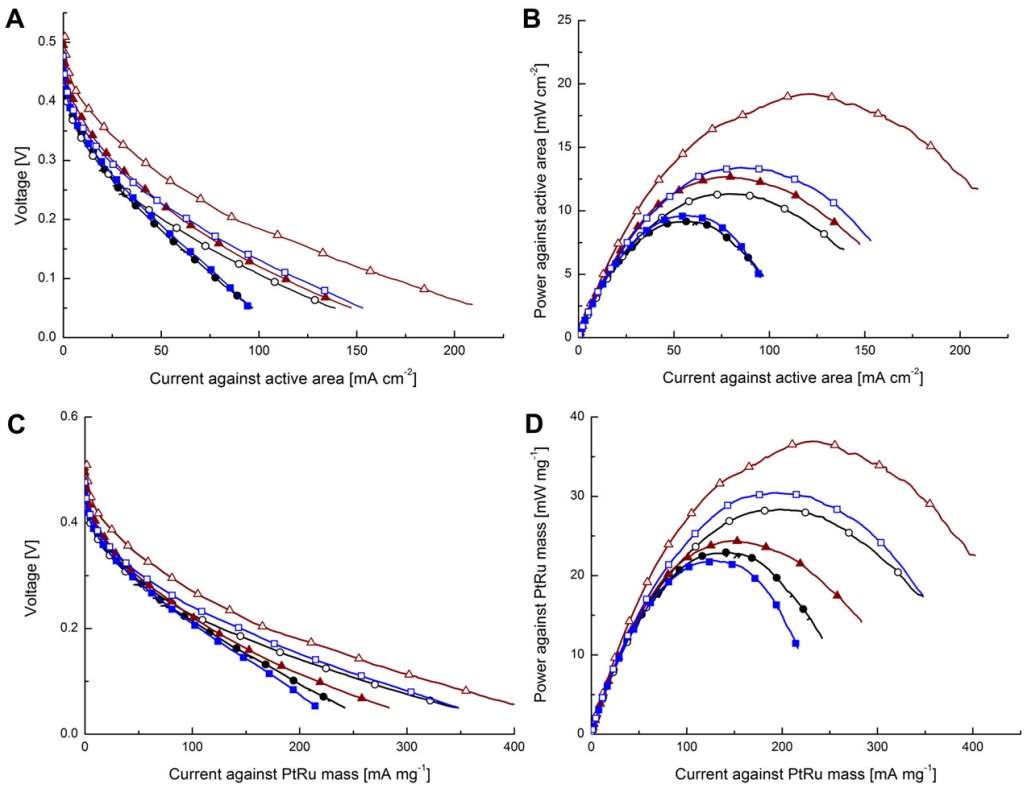

Fig. 5 – Performance of the different MEAs normalized against the (A, B) active area of the cell and (C, D) the mass of PtRu on the anode of the MEA. The black circles refer to MEA30, the red triangles to MEA50 and the blue squares to MEA70. The curves with filled symbols have been measured before the 9-day galvanostatic measurement and open symbols after. (For interpretation of the references to color in this figure legend, the reader is referred to the web version of this article.)

Table 2 – Performance of the DMFC equipped with different MEAs and the electrochemically active surface area of the anode before and after the 9-day galvanostatic measurement.

	P_{max}[a] (mW mg^{-1})		i @ 0.05 V[b] (mA mg^{-1})		OCV (V)		EASA (m^2 g^{-1})	
	Before	After	Before	After	Before	After	Before	After
MEA30	22.9	28.3	242	347	472	463	40.1	31.7
MEA50	24.4	36.9	283	402	495	509	42.5	39.4
MEA70	21.9	30.5	216	348	454	478	43.6	52.6

a Maximum power of the DMFC normalized against the anode PtRu mass.
b Current density at DMFC voltage of 0.05 V normalized against the anode PtRu mass.

the GNF. The increased mass transfer resistance of the thicker and more compact catalyst layer of MEA70 is only noticeable at high current density (Fig. 5C, D), whereas in MEA50 the layer has still enough pathways or voids to allow excellent performance. This may be caused by the macroporous 3D structure of the electrode visible in the SEM images (Fig. 3) or by a possible mesoporous structure of the GNF that enhances the transfer of reactants and products through the catalyst layer [17,18]. On the other hand, the visibly most porous electrode structure in MEA30 results in poorer performance than MEA50, which is probably due to the better conductivity of the catalyst layer in MEA50.

After the 9-day galvanostatic measurement, all the MEAs showed improved performance (Fig. 5C, D). From Table 2, it can be clearly seen that MEA50 (36.9 mW mg^{-1}) offers the best performance in terms of maximum power density followed by MEA70 (30.5 mW mg^{-1}) and then by MEA30 (28.3 mW mg^{-1}). These results reflect the changes during the 9-day measurement even though the absolute increase in maximum power is larger than expected but it can be explained by the mild activation procedure of the MEAs at OCV. The current densities at 0.05 V are now (in mA mg^{-1}): 347 (MEA30), 402 (MEA50) and 348 (MEA70). Even though the maximum power density is higher for MEA70 than for MEA30, the highest current densities are the same indicating that the high resistance and mass transfer limitations still affect the performance of MEA70. However, as the currents are much higher than before the 9-day measurement, it seems that the mass transfer has improved. This suggests that the anode catalyst layer has changed offering more pathways to methanol and/or CO_2 and other oxidation products. It may be possible that the gaseous CO_2 produced at the anode has penetrated through the catalyst layer and thus formed more pathways to the active sites. On the other hand, the overall structure of the catalyst layers has not changed visibly in the SEM images (Fig. 3A, F) meaning that the possible changes are very small and may be masked after the MEA has been removed from the fuel cell and prepared for the SEM imaging (freezing and cutting a sample).

Altogether, these results demonstrate that when GNF is used as the catalyst support, it is important to have a relatively large amount of Nafion in the catalyst layer to ensure a high and stable performance. As the previous reports [30–32] of the optimum DMFC anode Nafion content have lacked constant current testing over extended time periods and very high Nafion contents (>60 wt%), it is difficult to say if a similar performance enhancement at high Nafion content occurs with the traditional Vulcan black supported catalyst or if it is a property of the GNF support.

The electrochemically active surface area of the anode of each MEA has been determined before and after the 9-day galvanostatic measurement to elucidate the possible changes in the catalyst layer that are not visible in the SEM images. It has to be noted that due to changes in the humidification of the fuel cell and CO feeding during EASA determination, the results can only be used to compare individual MEAs before and after the 9-day measurement and not against each other. The changes in the active areas are comparable to the voltage drops during the 9-day measurements: the area decreases for MEA30 (−8.4 m^2 g^{-1}), decreases less for MEA50 (−3.9 m^2 g^{-1}) and increases for MEA70 (+9.0 m^2 g^{-1}). Usually, the active area decreases through fuel cell use [40], so in the case of MEA70, the growth of the active area with increased Nafion content can only be due to changes in the catalyst layer morphology that enable more PtRu particles to be accessible and active. Possible reasons for this include new pathways formed by CO_2 bubbles discussed above or swelling of Nafion by methanol so it comes into contact with more PtRu particles.

The change in the OCV supports the idea that the catalyst layer structure has more pathways after the 9-day galvanostatic measurement: it increases for MEA50 and MEA70, and decreases for MEA30 (Table 2). As OCV is mostly dependent on the concentration of species at the electrodes at constant temperature, it seems that after the 9-day measurement methanol has better access into the anode catalyst layer than before for MEA50 and MEA70. The reduced hydrophobicity of the layer supports this finding as methanol is a polar molecule. However, this does not increase the methanol crossover greatly as the larger methanol concentration on the cathode would decrease the OCV. This suggests that the methanol remains in the catalyst layer during DMFC usage, which could be due to an increased amount of pathways.

4. Conclusions

In this work, MEAs for a DMFC has been made with GNF-supported PtRu as the anode catalyst. The effect of Nafion content in the anode catalyst layer on stability and performance of the DMFC is studied at 30, 50 and 70 wt% Nafion to total catalyst layer mass (MEA30, MEA50, MEA70). During the whole course of experiments MEA50 showed the best performance reaching power densities of 19.2 mW cm^{-2} or 36.9 mW mg(PtRu)$^{-1}$. During a 9-day galvanostatic measurement MEA30 exhibited the lowest stability (−124 μV h^{-1}) while MEA50 is almost stable (−11 μV h^{-1}) and performance of MEA70 increased (+115 μV h^{-1}). Measurements of the

electrochemically active area show similar changes during the 9-day measurement for each MEA. As the optimum Nafion content of a commercial Vulcan carbon black supported PtRu anode of a DMFC is between 20 and 40 wt%, it can be said that the optimum electrode structure of GNF-supported anode is significantly larger and around 50 wt%. In this case, it seems that to form a continuous ion conductive network, the elongated shape of the GNF and porous catalyst layer structure requires more Nafion when compared with the compact layers formed with spherical carbon black. On the other hand, the porous 3D structure formed by the GNF in the catalyst layer can facilitate the mass transfer that would otherwise be limited by the large amount of Nafion.

This study underlines the importance of optimizing the electrode structure when new catalysts are studied in fuel cell conditions, otherwise their full potential may remain undiscovered. In addition, the real optimum structure can only be determined after long-term testing under fuel cell conditions as the stability of the MEA is strongly dependent on the electrode structure.

Acknowledgments

The authors would like thank the following instances for funding: MIDE and Starting Grant at Aalto University (P.K. and T.K.), Academy of Finland (V.R., Academy Research Fellowship, T.K., Postdoctoral Researcher, M.R.), the Spanish Ministry of Science and Innovation (V.R. Ramón y Cajal Programme). Ms. Tiia Viinikainen from the Aalto University Department of Biotechnology and Chemical Technology is gratefully acknowledged for arranging the possibility for the specific surface area measurements. Dr. Benjamin Wilson is gratefully acknowledged for proofreading the manuscript.

REFERENCES

[1] Zhao X, Yin M, Ma L, Liang L, Liu C, Liao J, Lu T, Xing W. Recent advances in catalysts for direct methanol fuel cells. Energy and Environmental Science 2011;4(8):2736–53.
[2] Ahmad H, Kamarudin SK, Hasran UA, Daud WRW. Overview of hybrid membranes for direct-methanol fuel-cell applications. International Journal of Hydrogen Energy 2010; 35(5):2160–75.
[3] Antolini E. Carbon supports for low-temperature fuel cell catalysts. Applied Catalysis B 2009;88(1–2):1–24.
[4] Kongkanand A, Vinodgopal K, Kuwabata S, Kamat PV. Highly dispersed Pt catalysts on single-walled carbon nanotubes and their role in methanol oxidation. Journal of Physical Chemistry B 2006;110(33):16185–8.
[5] Drillet J-F, Bueb H, Dittmeyer R, Dettlaff-Weglikowska U, Roth S. Efficient SWCNT-based anode for DMFC applications. Journal of the Electrochemical Society 2009; 156(10):F137–44.
[6] Wang X, Li W, Chen Z, Waje M, Yan Y. Durability investigation of carbon nanotube as catalyst support for proton exchange membrane fuel cell. Journal of Power Sources 2006;158(1):154–9.
[7] Li W, Liang C, Zhou W, Qiu J, Sun G, Xin Q. Preparation and characterization of multiwalled carbon nanotube-supported platinum for cathode catalysts of direct methanol fuel cells. Journal of Physical Chemistry B 2003;107(26):6292–9.
[8] Li L, Xing Y. Pt-Ru nanoparticles supported on carbon nanotubes as methanol fuel cell catalysts. Journal of Physical Chemistry C 2007;111(6):2803–8.
[9] Maiyalagan T. Pt–Ru nanoparticles supported PAMAM dendrimer functionalized carbon nanofiber composite catalysts and their application to methanol oxidation. Journal of Solid State Electrochemistry 2009;13(10):1561–6.
[10] Zhang Y, Jiang L, Li H, Fan L, Hu W, Wang C, Li Y, Yang S. Single-crystalline C60 nanostructures by sonophysical preparation: tuning hollow nanobowls as catalyst supports for methanol oxidation. Chemistry: A European Journal 2011; 17(17):4921–6.
[11] Xu B, Yang X, Wang X, Guo J, Liu X. A novel catalyst support for DMFC: onion-like fullerenes. Journal of Power Sources 2006;162(1):160–4.
[12] Kosaka M, Kuroshima S, Kobayashi K, Sekino S, Ichihashi T, Nakamura S, Yoshitake T, Kubo Y. Single-wall carbon nanohorns supporting Pt catalyst in direct methanol fuel cells. Journal of Physical Chemistry C 2009;113(20):8660–7.
[13] Salgado JRC, Alcaide F, Álvarez G, Calvillo L, Lázaro MJ, Pastor E. Pt–Ru electrocatalysts supported on ordered mesoporous carbon for direct methanol fuel cell. Journal of Power Sources 2010;195(13):4022–9.
[14] Maiyalagan T, Alaje TO, Scott K. Highly stable Pt–Ru nanoparticles supported on three-dimensional cubic ordered mesoporous carbon (Pt–Ru/CMK-8) as promising electrocatalysts for methanol oxidation. Journal of Physical Chemistry C 2012;116(3):2630–8.
[15] Serp P, Corrias M, Kalck P. Carbon nanotubes and nanofibers in catalysis. Applied Catalysis A 2003;253(2):337–58.
[16] Endo M, Kim Y, Hayashi T, Nishimura K, Matusita T, Miyashita K, Dresselhaus M. Vapor-grown carbon fibers (VGCFS) – basic properties and their battery applications. Carbon 2001;39(9):1287–97.
[17] Calvillo L, Gangeri M, Perathoner S, Centi G, Moliner R, Lázaro MJ. Effect of the support properties on the preparation and performance of platinum catalysts supported on carbon nanofibers. Journal of Power Sources 2009;192(1):144–50.
[18] Sebastián D, Calderón JC, González-Expósito JA, Pastor E, Martínez-Huerta MV, Suelves I, Moliner R, Lázaro MJ. Influence of carbon nanofiber properties as electrocatalyst support on the electrochemical performance for PEM fuel cells. International Journal of Hydrogen Energy 2010;35(18): 9934.
[19] Kang S, Lim S, Peck D-H, Kim S-K, Jung D-H, Hong S-H, Jung H-G, Shul Y. Stability and durability of PtRu catalysts supported on carbon nanofibers for direct methanol fuel cells. International Journal of Hydrogen Energy 2012;37(5): 4685–93.
[20] Kim T, Lim S, Kwon K, Hong S-H, Qiao W, Rhee CK, Yoon S-H, Mochida I. Electrochemical capacitances of well-defined carbon surfaces. Langmuir 2006;22(22):9086–8.
[21] Bessel CA, Laubernds K, Rodriguez NM, Baker RTK. Graphite nanofibers as an electrode for fuel cell applications. Journal of Physical Chemistry B 2001;105(6):1115–8.
[22] Wang D, Liu Y, Huang J, You T. In situ synthesis of Pt/carbon nanofiber nanocomposites with enhanced electrocatalytic activity toward methanol oxidation. Journal of Colloid and Interface Science 2012;367(1):199–203.
[23] Santasalo-Aarnio A, Borghei M, Anoshkin IV, Nasibulin AG, Kauppinen EI, Ruiz V, Kallio T. Durability of different carbon nanomaterial supports with PtRu catalyst in a direct methanol fuel cell. International Journal of Hydrogen Energy 2012;37(4):3415–24.
[24] Steigerwalt ES, Deluga GA, Lukehart CM. Pt–Ru/carbon fiber nanocomposites: synthesis, characterization, and

performance as anode catalysts of direct methanol fuel cells. a search for exceptional performance. Journal of Physical Chemistry B 2002;106(4):760–6.
[25] Guo J, Sun G, Wang Q, Wang G, Zhou Z, Tang S, Jiang L, Zhou B, Xin Q. Carbon nanofibers supported Pt–Ru electrocatalysts for direct methanol fuel cells. Carbon 2006; 44(1):152–7.
[26] Tsuji M, Kubokawa M, Yano R, Miyamae N, Tsuji T, Jun M-S, Hong S, Lim S, Yoon S-H, Mochida I. Fast preparation of PtRu catalysts supported on carbon nanofibers by the microwave-polyol method and their application to fuel cells. Langmuir 2007;23(2):387–90.
[27] Okada M, Konta Y, Nakagawa N. Carbon nano-fiber interlayer that provides high catalyst utilization in direct methanol fuel cell. Journal of Power Sources 2008;185(2): 711–6.
[28] Park S-M, Jung D-H, Kim S-K, Lim S, Peck D, Hong WH. The effect of vapor-grown carbon fiber as an additive to the catalyst layer on the performance of a direct methanol fuel cell. Electrochimica Acta 2009;54(11):3066–72.
[29] Kim J-H, Ha HY, Oh I-H, Hong S-A, Kim HN, Lee H-I. Electrochemical studies of DMFC anodes with different ionomer content. Electrochimica Acta 2004;50(2–3):801–6.
[30] Krishnamurthy B, Deepalochani S, Dhathathreyan KS. Effect of ionomer content in anode and cathode catalyst layers on direct methanol fuel cell performance. Fuel Cells 2008;8(6): 404–9.
[31] Birry L, Bock C, Xue X, McMillan R, MacDougall B. DMFC electrode preparation, performance and proton conductivity measurements. Journal of Applied Electrochemistry 2009; 39(3):347–60.
[32] Wannek C, Nehr S, Vahlenkamp M, Mergel J, Stolten D. Pseudo-half-cell measurements on symmetrical catalyst-coated membranes and their relevance for optimizing DMFC anodes. Journal of Applied Electrochemistry 2010;40(1): 29–38.
[33] Thomas SC, Ren X, Gottesfeld S. Influence of ionomer content in catalyst layers on direct methanol fuel cell performance. Journal of the Electrochemical Society 1999; 146(12):4354–9.
[34] Dohle H, Schmitz H, Bewer T, Mergel J, Stolten D. Development of a compact 500 W class direct methanol fuel cell stack. Journal of Power Sources 2002;106(1–2):313–22.
[35] Zhao X, Fan X, Wang S, Yang S, Yi B, Xin Q, Sun G. Determination of ionic resistance and optimal composition in the anodic catalyst layers of DMFC using AC impedance. International Journal of Hydrogen Energy 2005;30(9):1003–10.
[36] Abdelkareem MA, Tsujiguchi T, Nakagawa N. Effect of black catalyst ionomer content on the performance of passive DMFC. Journal of Power Sources 2010;195(19):6287–93.
[37] Jeng K-T, Chien C-C, Hsu N-Y, Huang W-M, Chiou S-D, Lin S-H. Fabrication and impedance studies of DMFC anode incorporated with CNT-supported high-metal-content electrocatalyst. Journal of Power Sources 2007;164(1):33–41.
[38] Li W, Waje M, Chen Z, Larsen P, Yan Y. Platinum nanopaticles supported on stacked-cup carbon nanofibers as electrocatalysts for proton exchange membrane fuel cell. Carbon 2010;48(4):995–1003.
[39] Goswami S, Klaus S, Benziger J. Wetting and absorption of water drops on Nafion films. Langmuir 2008;24(16):8627–33.
[40] Wang Z-B, Wang X-P, Zuo P-J, Yang B-Q, Yin G-P, Feng X-P. Investigation of the performance decay of anodic PtRu catalyst with working time of direct methanol fuel cells. Journal of Power Sources 2008;181(1):93–100.
[41] Leger J-M, Beden B, Lamy C, Bilmes S. Carbon monoxide electrosorption on low index platinum single crystal electrodes. Journal of Electroanalytical Chemistry and Interfacial Electrochemistry 1984;170(1–2):305–17.
[42] Liu J, Zhou Z, Zhao X, Xin Q, Sun G, Yi B. Studies on performance degradation of a direct methanol fuel cell (DMFC) in life test. Physical Chemistry Chemical Physics 2004;6(1):134–7.
[43] Showa Denko [Internet]. Vapor grown carbon nanofiber. [accessed 3.7.2012]. Available from: http://www.sdkc.com/documents/VGCF-H.pdf.
[44] Slade S, Campbell SA, Ralph TR, Walsh FC. Ionic conductivity of an extruded Nafion 1100 EW series of membranes. Journal of the Electrochemical Society 2002;149(12):A1556–64.
[45] Lee J-H, Paik U, Choi J-Y, Kim KK, Yoon S-M, Lee J, Kim B-K, Kim JM, Park MH, Yang CW, An KH, Lee YH. Dispersion stability of single-walled carbon nanotubes using Nafion in bisolvent. Journal of Physical Chemistry C 2007;111(6): 2477–83.
[46] Yu HM, Ziegler C, Oszcipok M, Zobel M, Hebling C. Hydrophilicity and hydrophobicity study of catalyst layers in proton exchange membrane fuel cells. Electrochimica Acta 2006;51(7):1199–207.
[47] Brack H-P, Slaski M, Gubler L, Scherer GG, Alkan S, Wokaun A. Characterisation of fuel cell membranes as a function of drying by means of contact angle measurements. Fuel Cells 2004;4(3):141–6.
[48] Cha H-C, Chen C-Y, Shiu J-Y. Investigation on the durability of direct methanol fuel cells. Journal of Power Sources 2009; 192(2):451–6.
[49] Park Y-C, Peck D-H, Kim S-K, Lim S, Jung D-H, Jang J-H, Lee D-Y. Dynamic response and long-term stability of a small direct methanol fuel cell stack. Journal of Power Sources 2010;195(13): 4080–9.
[50] Nakagawa N, Xiu Y. Performance of a direct methanol fuel cell operated at atmospheric pressure. Journal of Power Sources 2003;118(1–2):248–55.